Electronic structure and optical gain saturation of $InAs_{1-x}N_x/GaAs$ quantum dots

J. Chen,[1] W. J. Fan,[1,a)] Q. Xu,[1] X. W. Zhang,[1] S. S. Li,[2] and J. B. Xia[2]
[1]School of Electrical and Electronic Engineering, Nanyang Technological University, Singapore 639798, Singapore
[2]Institute of Semiconductors, Chinese Academy of Sciences, P.O. Box 912, Beijing 10083, China

(Received 3 November 2008; accepted 4 May 2009; published online 17 June 2009)

The electronic band structures and optical gains of $InAs_{1-x}N_x/GaAs$ pyramid quantum dots (QDs) are calculated using the ten-band $\mathbf{k}\cdot\mathbf{p}$ model and the valence force field method. The optical gains are calculated using the zero-dimensional optical gain formula with taking into consideration of both homogeneous and inhomogeneous broadenings due to the size fluctuation of quantum dots which follows a normal distribution. With the variation of QD sizes and nitrogen composition, it can be shown that the nitrogen composition and the strains can significantly affect the energy levels especially the conduction band which has repulsion interaction with nitrogen resonant state due to the band anticrossing interaction. It facilitates to achieve emission of longer wavelength (1.33 or 1.55 μm) lasers for optical fiber communication system. For QD with higher nitrogen composition, it has longer emission wavelength and less detrimental effect of higher excited state transition, but nitrogen composition can affect the maximum gain depending on the factors of transition matrix element and the Fermi–Dirac distributions for electrons in the conduction bands and holes in the valence bands respectively. For larger QD, its maximum optical gain is greater at lower carrier density, but it is slowly surpassed by smaller QD as carrier concentration increases. Larger QD can reach its saturation gain faster, but this saturation gain is smaller than that of smaller QD. So the trade-off between longer wavelength, maximum optical, saturation gain, and differential gain must be considered to select the appropriate QD size according to the specific application requirement.
© *2009 American Institute of Physics*. [DOI: 10.1063/1.3143025]

I. INTRODUCTION

The self-assembled InAs quantum dots (QDs) grown on GaAs have received great attention due to their applications in the next generation of telecommunication optoelectronic devices such as lasers.[1,2] A lot of efforts have been done to expand the emission wavelength toward 1.3 μm by embedding the QDs into an InGaAs quantum well or stacking of QDs.[3,4] Another way is to substitute small amount of nitrogen atoms into the QD,[5,6] after discovery of strong negative band gap bowing effects in dilute nitride semiconductor.[7] The progress in the fabrication techniques of dilute nitride QD facilitates the realization of the 1.3 μm optical fiber communication laser, it is even possible to reach 1.55 μm.[8] Theoretically, it is found that when the doped nitrogen atoms replace a small amount of the As atoms, it reduces the energy gap and increases the electron effective mass in the conduction band.[9] This can be explained by the repulsion between the conduction band edge and a higher-lying nitrogen resonant state.[10] The doped nitrogen can also reduce the lattice constant of QDs, resulting in reducing the compressive strain formed due to the lattice mismatch which is one possible reason for the degradation of lasers.[11,12]

InAsN/GaAs QDs can provide longer wavelength emission and other better characteristics than InAs/GaAs QDs. Therefore, it has greater potential to fabricate advanced GaAs-based optical fiber communication lasers which are capable of large gain and large output power. But if the nitrogen composition is too high, the excessive nitrogen atoms may act as nonradiative recombination centers resulting in reduction of optical gain. In this paper, we apply ten-band $k\cdot p$ model which includes the coupled conduction and valence bands, and orbit-splitting and nitrogen bands to study the electronic structure and optical gain saturation in InAsN/GaAs QDs. As strain is a significant factor, we calculate the strain using the valence force field (VFF) model. We take into account both homogeneous and inhomogeneous broadening for the optical gain spectrum.[13] The homogeneous broadening with width of a single dot is proportional to the polarization dephasing rate, while the inhomogeneous broadening of the quantized energies is duo to size fluctuation of the QDs. Then we present the comparison of optical gain among nitrogen-added and nitrogen-free QDs and the effect of different QDs size and different carrier density on the optical gain.

II. THEORETICAL MODEL

The conventional eight-band $k\cdot p$ method cannot be applied directly to nitrogen-doped QDs, because the strong interaction between the nitrogen resonant states and the conduction band edge must be considered.[14,15] Based on the band anticrossing model, the electronic structures and optical properties are calculated by a ten-band $k\cdot p$ model which includes the additional two spin-degenerated nitrogen-related energy levels. The ten-band Hamiltonian is represented in the

a)Electronic mail: ewjfan@ntu.edu.sg.

 © 2009 American Institute of Physics

Author complimentary copy. Redistribution subject to AIP license or copyright, see http://jap.aip.org/jap/copyright.jsp

Bloch function basis $|S\rangle\uparrow$, $|11\rangle\uparrow$, $|10\rangle\uparrow$, $|1-1\rangle\uparrow$, $|S_N\rangle\uparrow$, $|S\rangle\downarrow$, $|11\rangle\downarrow$, $|10\rangle\downarrow$, $|1-1\rangle\downarrow$, $|S_N\rangle\downarrow$ as

$$H_{\text{ten}} = \begin{pmatrix} H_{\text{int}} & 0 \\ 0 & H_{\text{int}} \end{pmatrix} + H_{\text{so}} + V_0, \tag{1}$$

where $|S_N\rangle$ is the basis of the nitrogen, H_{so} is the valence band spin-orbit coupling Hamiltonian, V_0 is the confining potential of the QD which is zero in the dot and finitely high in the barrier, and H_{int} contains all the k-independent, k-linear, and k-quadratic terms. H_{int} can be written as[16]

$$H_{\text{int}} = \begin{pmatrix} E_g + P_e & \frac{i}{\sqrt{2}}p_0(k_x' + ik_y') & ip_0k_z' & \frac{i}{\sqrt{2}}p_0(k_x' - ik_y') & V_{\text{NC}}\sqrt{x} \\ -\frac{i}{\sqrt{2}}p_0(k_x' - ik_y') & P_1 & S & T & 0 \\ -ip_0k_z' & S^* & P_3 & S & 0 \\ -\frac{i}{\sqrt{2}}p_0(k_x' + ik_y') & T^* & S^* & P_1 & 0 \\ V_{\text{NC}}\sqrt{x} & 0 & 0 & 0 & E_N \end{pmatrix}, \tag{2}$$

where E_g is the band gap of bulk material, $p_0=\hbar\sqrt{E_p/2m_0}$, E_p is the matrix element of Kane's theory, $E_{\text{N}}=1.44$ eV is the nitrogen energy level relative to the valence band maximum of InAs, $V_{\text{NC}}=2.0$ eV is the coupling strength between conduction band and nitrogen energy level,[16] and x is the composition of the nitrogen in InAs and

$$k_x' = k_x - \varepsilon_{xx}k_x - \varepsilon_{xy}k_y - \varepsilon_{xz}k_z, \tag{3a}$$

$$k_y' = k_y - \varepsilon_{xy}k_x - \varepsilon_{yy}k_y - \varepsilon_{yz}k_z, \tag{3b}$$

$$k_z' = k_z - \varepsilon_{xz}k_x - \varepsilon_{yz}k_y - \varepsilon_{zz}k_z, \tag{3c}$$

$$P_e = \frac{\hbar^2}{2m_0}\gamma_c(k_x^2 + k_y^2 + k_z^2) + a_c(\varepsilon_{xx} + \varepsilon_{yy} + \varepsilon_{zz}), \tag{3d}$$

$$P_1 = -\frac{\hbar^2}{2m_0}\left[\frac{L' + M'}{2}(k_x^2 + k_y^2) + M'k_z^2\right] + \left(a_v + \frac{b}{2}\right)(\varepsilon_{xx} + \varepsilon_{yy}) + (a_v - b)\varepsilon_{zz}, \tag{3e}$$

$$P_3 = -\frac{\hbar^2}{2m_0}[M'(k_x^2 + k_y^2) + L'k_z^2] + (a_v - b)(\varepsilon_{xx} + \varepsilon_{yy}) + (a_v + 2b)\varepsilon_{zz}, \tag{3f}$$

$$S^* = -\frac{\hbar^2}{2m_0}\left[\frac{1}{\sqrt{2}}N'(k_x + ik_y)k_z\right] + \sqrt{6}d(\varepsilon_{xz} + i\varepsilon_{yz}), \tag{3g}$$

$$T^* = -\frac{\hbar^2}{2m_0}\left[\frac{L' - M'}{2}(k_x^2 - k_y^2) + iN'k_xk_y\right] + \frac{3}{2}b(\varepsilon_{xx} - \varepsilon_{yy}) + i2\sqrt{3}d\varepsilon_{xy}, \tag{3h}$$

where ε_{xx}, ε_{yy}, ... are the strain components, a_c and a_v are the hydrostatic deformation potentials of conduction band and valence band of the host material, b and d are the shear deformation potentials along the [001] and [111] direction of the host material, γ_c, L', M', N' are given by $\gamma_c=(m_0/m_c) -(E_p/3)((2/E_g)+(1/E_g+3\lambda))$, $L'=L-E_p/E_g$, $M'=M$, $N'=N-E_p/E_g$, where m_c is the electron effective mass, λ is the spin-orbit coefficient, $\lambda=\Delta_{\text{so}}/3$, Δ_{so} is the spin-orbit splitting energy, and L, M and N are the Luttinger parameters. For InAs, $m_c=0.022\,26m_0$, $L=53.13$, $M=2.93$, $N=55.74$, and $E_P=22.2$ eV.[17] The conduction band offset is assumed to be 70% of the band gap difference.[18] The other parameters of InAs and GaAs are listed in Table I.[17,19]

H_{so} can be written as[20]

TABLE I. Parameters of InAs and GaAs used in the calculation (Refs. 17 and 19).

Material	a_0 (nm)	E_g (eV)	Δ_{so} (eV)	a_c (eV)	a_v (eV)	b (eV)	d (eV)
InAs	0.605 83	0.354	0.38	−5.08	1.0	−1.8	−3.6
GaAs	0.565 33	1.424	0.341	−7.17	1.16	−1.7	−4.55

Author complimentary copy. Redistribution subject to AIP license or copyright, see http://jap.aip.org/jap/copyright.jsp

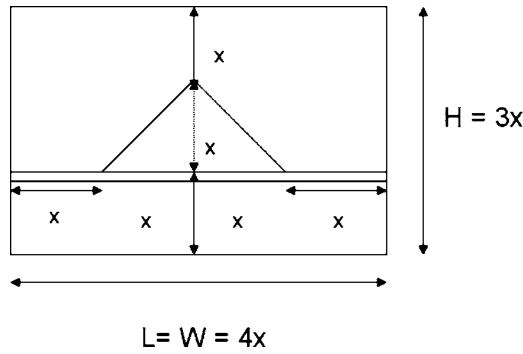

FIG. 1. Schematic of a square pyramidal InAs dot with side view. The height (H) and the width (L or W) of the unit cell are three and four times of the height of QD, respectively.

$$H_{so}=\begin{pmatrix} 0&0&0&0&0&0&0&0&0&0\\ 0&0&0&0&0&0&0&0&0&0\\ 0&0&-\lambda&0&0&0&-\sqrt{2}\lambda&0&0&0\\ 0&0&0&-2\lambda&0&0&0&\sqrt{2}\lambda&0&0\\ 0&0&0&0&0&0&0&0&0&0\\ 0&0&0&0&0&0&0&0&0&0\\ 0&0&-\sqrt{2}\lambda&0&0&0&-2\lambda&0&0&0\\ 0&0&0&\sqrt{2}\lambda&0&0&0&-\lambda&0&0\\ 0&0&0&0&0&0&0&0&0&0\\ 0&0&0&0&0&0&0&0&0&0 \end{pmatrix}. \quad (4)$$

We assume that the dots are three dimensionally and periodically arranged. The periodicities are L_x, L_y, and L_z. The ten-dimensional electron and hole envelope wave function for the quantum dots can be expressed as

$$\Phi_m=\{\Phi_m^j\}(j=1,2,\ldots,10), \quad (5)$$

$$\Phi_m^j=\frac{1}{\sqrt{L_xL_yL_z}}\sum_{n_x,n_y,n_z} a^j_{m,n_x,n_y,n_z}\exp[i(k_{nx}x+k_{ny}y+k_{nz}z)], \quad (6)$$

where $k_{nx}=k_{x0}+(2\pi/L_x)n_x$, $k_{ny}=k_{y0}+(2\pi/L_y)n_y$, and $k_{nz}=k_{z0}+(2\pi/L_z)n_z$, k_{x0}, k_{y0}, and k_{z0} represent the wave vectors of the dot ensemble. We set $k_{x0}=k_{y0}=k_{z0}=0$. The n_x, n_y, and n_z are the integers of plane wave numbers in the range of ± 3, m is the index for energy subbands, and j is the index for basis. The matrix is solved by direct diagonalization.

For InAsN/GaAs pyramid QD, we assume that the pyramid axis is along the direction of positive z direction, and the two-monolayer wetting layer is in the x-y plane. Every surface of the pyramid is a simple crystal plane, and the pyramid base width (b_s) is twice of the height (x). The fixed dimension ratio of QDs is shown in Fig. 1.

The lattice-mismatch induced strain distribution is considered and calculated by using the VFF model which is a microscopic theory considering both bond stretching and bond bending in the calculation. The total VFF energy is taken as[21]

TABLE II. Parameters of InAsN and GaAs used in VFF calculation (Refs. 21–23).

	Bond distance d^0_{ij} (Å)	$\alpha(10^3$ dyne/cm)
In–As	2.623 321	35.180
Ga–As	2.447 929	41.190
In–N	2.156	79.200
Ga–N	1.949	96.300

	$\beta(10^3$ dyne/cm)		$\beta(10^3$ dyne/cm)
As–In–As	5.488 08	In–As–In	5.488 08
As–Ga–As	8.938 23	Ga–As–Ga	8.938 23
N–In–N	7.100 00	In–N–In	7.100 00
N–Ga–N	14.800 0	Ga–N–Ga	14.800 0
Ga–N–In	10.950 0	N–In–As	6.294 040
N–Ga–As	11.869 115	Ga–As–In	7.213 155

$$V=\frac{1}{4}\sum_{ij}\frac{3}{4}\alpha_{ij}(d_{ij}^2-d_{0,ij}^2)^2/d_{0,ij}^2 + \frac{1}{2}\sum_i\sum_{j\neq k}\frac{3}{4}\beta_{ijk}(\Re_{ij}\bullet\Re_{ik}+d_{0,ij}d_{0,ik}/3)^2/d_{0,ij}d_{0,ik}, \quad (7)$$

where i runs over all the atomic sites, j *and* k run over the nearest-neighbor sites of i, $\Re_{ij}$ is the vector joining the sites i and j, d_{ij} denotes the length of the bond, $d_{0,ij}$ denotes the corresponding equilibrium length in the binary constituents, and α_{ij} and β_{ijk} are the bond stretching and bond bending constants, respectively.[21] The parameters used in VFF calculation are listed in Table II.[21–23] The detailed process of calculation is in Refs. 21–23.

The formulas for the optical gain spectrum are presented, taking into account both homogeneous and inhomogeneous broadening. Based on the density-matrix equation, the optical gain spectra showing homogeneous broadening is calculated as[13]

$$G(E)=\frac{\pi e^2\hbar}{m_0^2\varepsilon_0 n_r cE}\sum_{n_c,n_v}\frac{1}{V}|M^{cv}|^2[f_c+f_v-1]\times\frac{1}{\pi}\times B_{cv}(E-E_{cv}), \quad (8)$$

where E is the photon energy, e is the electron charge, ε_0 is the free-space dielectric constant, n is the refractive index, c is the speed of light, E_{cv} is the transition energy, and f_c and f_v are the Fermi–Dirac distributions for electrons in the conduction bands and holes in the valence bands, respectively.

$$f_c=\frac{1}{1+\exp[(E_{nc}-E_{fc})/k_BT]}, \quad (9a)$$

$$f_v=\frac{1}{1+\exp[(E_{nv}-E_{fv})/k_BT]}, \quad (9b)$$

where E_{nc} and E_{nv} are the quantized electron and hole energy levels, respectively, E_{fc} and E_{fv} are the electron and hole quasi-Fermi level, respectively, M^{cv} is the optical transition matrix element, and the squared optical transition matrix el-

Author complimentary copy. Redistribution subject to AIP license or copyright, see http://jap.aip.org/jap/copyright.jsp

ements measure the momentum of the transition between the hole subbands and the electron subbands.[24]

$$M_i^{cv} = \langle \Psi_{n_v,k} | \hat{p}_i | \Psi_{n_c,k} \rangle, \quad i = x,y,z, \tag{10}$$

where $\hat{p}_i$ is the momentum operator, $\Psi_{n_c,k}$ and $\Psi_{n_v,k}$ are the real electron and hole wave functions, respectively. The real wave function is the product of the envelope wave functions in Eq. (5) and the Bloch wave functions basis. The final expression for optical transition matrix element in the X, Y, and Z directions are

$$\begin{aligned} M_x^{cv} &= \langle \Psi_{n_v,k} | \hat{p}_x | \Psi_{n_c,k} \uparrow \rangle + \langle \Psi_{n_v,k} | \hat{p}_x | \Psi_{n_c,k} \downarrow \rangle \\ &= p_0 \sum_{n_x,n_y,n_z} \left[\frac{1}{\sqrt{2}} (a^2_{v,n_x,n_y,n_z} + a^4_{v,n_x,n_y,n_z}) a^{1*}_{c,n_x,n_y,n_z} \right. \\ &\quad + \frac{1}{\sqrt{2}} (a^7_{v,n_x,n_y,n_z} + a^9_{v,n_x,n_y,n_z}) a^{6*}_{c,n_x,n_y,n_z} \\ &\quad + \frac{1}{\sqrt{2}} (a^{2*}_{c,n_x,n_y,n_z} + a^{4*}_{c,n_x,n_y,n_z}) a^1_{v,n_x,n_y,n_z} \\ &\quad \left. + \frac{1}{\sqrt{2}} (a^{7*}_{c,n_x,n_y,n_z} + a^{9*}_{c,n_x,n_y,n_z}) a^6_{v,n_x,n_y,n_z} \right], \end{aligned} \tag{11}$$

$$\begin{aligned} M_y^{cv} &= \langle \Psi_{n_v,k} | \hat{p}_y | \Psi_{n_c,k} \uparrow \rangle + \langle \Psi_{n_v,k} | \hat{p}_y | \Psi_{n_c,k} \downarrow \rangle \\ &= p_0 \sum_{n_x,n_y,n_z} \left[\frac{i}{\sqrt{2}} (a^2_{v,n_x,n_y,n_z} - a^4_{v,n_x,n_y,n_z}) a^{1*}_{c,n_x,n_y,n_z} \right. \\ &\quad + \frac{i}{\sqrt{2}} (a^7_{v,n_x,n_y,n_z} - a^9_{v,n_x,n_y,n_z}) a^{6*}_{c,n_x,n_y,n_z} \\ &\quad + \frac{i}{\sqrt{2}} (a^{2*}_{c,n_x,n_y,n_z} - a^{4*}_{c,n_x,n_y,n_z}) a^1_{v,n_x,n_y,n_z} \\ &\quad \left. + \frac{i}{\sqrt{2}} (a^{7*}_{c,n_x,n_y,n_z} - a^{9*}_{c,n_x,n_y,n_z}) a^6_{v,n_x,n_y,n_z} \right], \end{aligned}$$

$$\begin{aligned} M_z^{cv} &= \langle \Psi_{n_v,k} | \hat{p}_z | \Psi_{n_c,k} \uparrow \rangle + \langle \Psi_{n_v,k} | \hat{p}_z | \Psi_{n_c,k} \downarrow \rangle \\ &= p_0 \sum_{n_x,n_y,n_z} [a^3_{v,n_x,n_y,n_z} a^{1*}_{c,n_x,n_y,n_z} + a^8_{v,n_x,n_y,n_z} a^{6*}_{c,n_x,n_y,n_z} \\ &\quad + a^{3*}_{c,n_x,n_y,n_z} a^1_{v,n_x,n_y,n_z} + a^{8*}_{c,n_x,n_y,n_z} a^6_{v,n_x,n_y,n_z}], \end{aligned}$$

where $p_0 = \langle S|p_x|X\rangle = \langle S|p_y|Y\rangle = \langle S|p_z|Z\rangle$. The x and y directions are symmetrical, we take the average of x and y direction to calculate the optical transition matrix element for the transverse electric (TE) mode, and the TE mode (polarized in the x direction) optical gain is calculated by taking the average of gains in the x and y directions. The optical transition matrix element in the z direction indicates the transverse magnetic (TM) mode, and the TM mode optical gain is polarized in the z direction. We assume the transition matrix element between the nitrogen S state and the valence band state is zero.

The homogeneous broadening of a Lorentz shape can be written as[13]

$$B_{cv}(E - E_{cv}) = \frac{\hbar/\tau}{(E - E_{cv})^2 + (\hbar/\tau)^2}, \tag{12}$$

where τ is the intraband relaxation time

In the actual QD lasers, we must take into account inhomogeneous broadening due to the size fluctuation of QDs in terms of the convolution integral as[13]

$$\begin{aligned} G(E) &= \frac{\pi e^2 \hbar}{m_0^2 \varepsilon_0 n_r c E} \sum_{n_c,n_v} \frac{1}{V} |M^{cv}|^2 \int_{-\infty}^{\infty} [f_c + f_v - 1] \\ &\quad \times \frac{1}{\pi} \times G(E' - E_{cv}) B_{cv}(E - E') dE', \end{aligned} \tag{13}$$

where the energy fluctuation of dots is represented by $G(E'\text{-}E_{cv})$, E_{cv} is the center of the energy distribution function of each interband transition. We take a Gaussian distribution function as[13]

$$G(E - E_{cv}) = \frac{1}{\sqrt{2\pi\sigma}} \exp[-(E - E_{cv})^2/(2\sigma^2)]. \tag{14}$$

Equation (13) indicates the optical gain at a given energy E which is created by collecting the individual contribution of all dots within the homogeneous broadening around the energy. If the homogeneous broadening is a δ function, i.e., $B_{cv}(E) = \delta(E)$, then Eq. (13) is reduced as[13]

$$\begin{aligned} G(E) &= \frac{\pi e^2 \hbar}{m_0^2 \varepsilon_0 n_r c E} \sum_{n_c,n_v} \frac{1}{V} |M^{cv}|^2 [f_c + f_v - 1] \\ &\quad \times \frac{1}{\pi} \times G(E - E_{cv}). \end{aligned} \tag{15}$$

In this case, dots with different energies have no correlation to each other and give optical gain independently since they are spatially isolated from each other.[25] In our calculation, we take the inhomogeneous broadening $\sigma = 20$ meV.[13,26] All our calculation are done at $T = 300$ K as room temperature is preferred for device to perform. Other parameters are taken from Ref. 19.

III. RESULTS AND DISCUSSION

The sizes of QDs and the nitrogen compositions are varied to investigate their influence on the electronic structure and optical properties. The QDs consist the ones with height x of 14, 18, 22, and 23 lattice constants (their actual lengths are 7.91, 10.2, 12.4, and 13.0 nm, respectively, and we call these structures H14, H18, H22, and H23 for convenience).

When nitrogen atoms substitute the As atoms, the compressive strain in QDs decreases. In order to consider this variation, in our simulation, we distribute nitrogen atoms uniformly in QD (including wetting layer) that every layer of QD has equal density of nitrogen atom shown in Fig. 2. Figure 2(a) shows in the x-y plane, N atoms are distributed uniformly, and Fig. 2(b) shows the side view of atoms distribution in QD and wetting layer.

At the location of nitrogen, the compressive strain is less than that in As atom. The strain distributions for H18 sized QD with 1% nitrogen atoms are shown in Figs. 3 and 4. Figure 3 shows the strain distribution profiles in two-

Author complimentary copy. Redistribution subject to AIP license or copyright, see http://jap.aip.org/jap/copyright.jsp

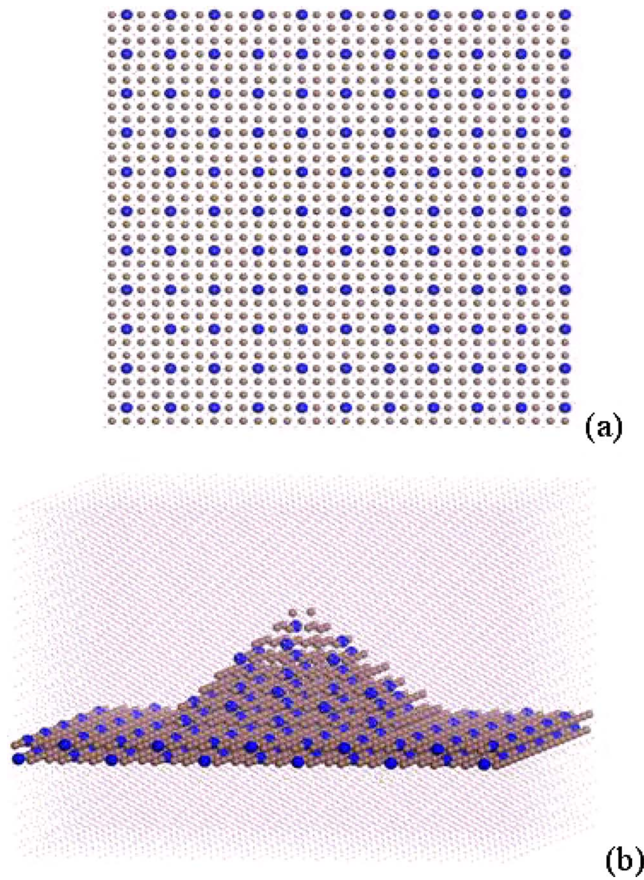

FIG. 2. (Color online) The top view and side view of the nitrogen distribution in QD and wetting layer. The blue atoms are nitrogen atoms.

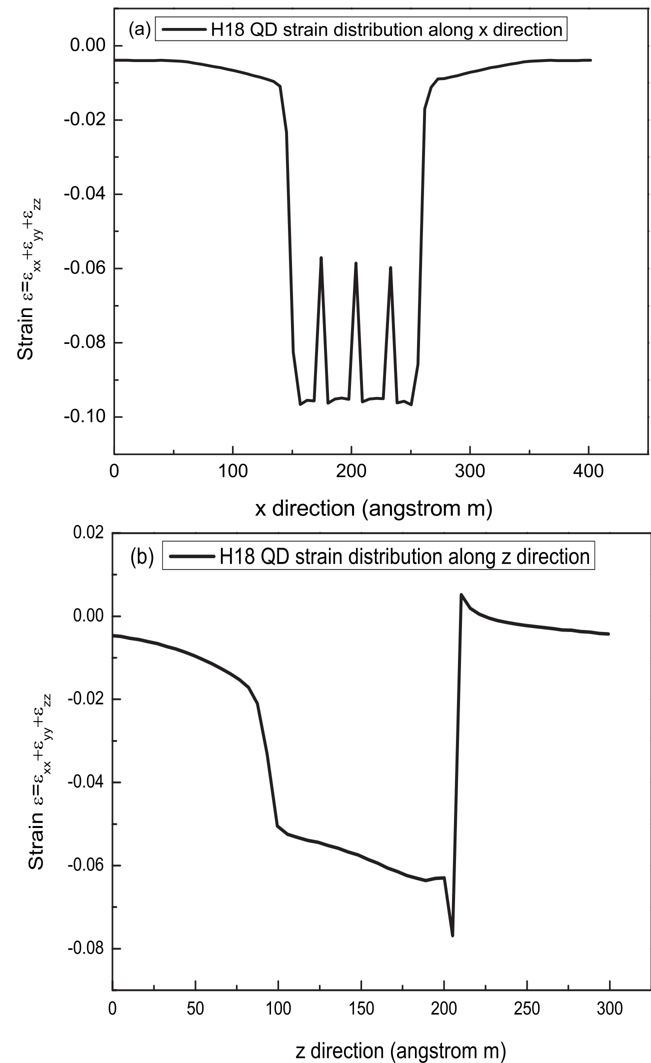

FIG. 3. The 2D strain distribution in the unit cell for H18 sized QD with 1% nitrogen composition in two dimensions (a) along the x direction (x and y are symmetrical) (b) along the z direction.

dimensional (2D) graphs. The strain is the sum of $\varepsilon_{xx}+\varepsilon_{yy}+\varepsilon_{zz}$. As the x and y directions are symmetrical, we show the strain in x and z directions in Figs. 3(a) and 3(b), respectively. Figure 3(a) shows that the strain inside InAsN is compressive (negative strain value) but at the location of N atoms, the compressive strain has smaller amplitude. In Fig. 3(b), as strain values are all taken from the middle of the squared base along the z direction, the compressive strain is smaller than InAs. Figure 4 shows the strain distribution profiles in three-dimensional (3D) graphs with two different view angles on the x-y and x-z planes, respectively. Figure 4(a) shows the x-y plane in the middle of the total height, so the wetting layer is not included in that plane. In the center (QD region) N atoms are mixed inside QD, and small peaks appear at the site of nitrogen. It shows the compressive strain at N atom is smaller than its nearest neighboring As atoms. The rest is barrier region which has very small strains which is almost 0. Figure 4(b) shows the x-z plane in the middle of total y dimension. It shows the compressive strain inside QD is greater than the compressive strains induced from N locations in QD and wetting layer. Compared to the N-free QD, this decrease of compressive strain inside QD can affect our calculation of energy band quite significantly.

Figure 5 shows the transition energy from cl (the first excited electron state) to hh1 (the first excited state of heavy hole) as a function of QDs height for different nitrogen compositions. When the size is increased, the valence band energy levels decrease slightly, but the conduction band energy levels decrease more rapidly. The reduction of effective c1-hh1 transition is contributed by the reduction in conduction band energy level. Another important factor is the strain which can modify the band structure via the deformation potentials.[27] The decrease in the conduction band is almost directly proportional to the nitrogen compositions. It implies the more added nitrogen atoms, the stronger repulsion interaction between nitrogen resonant level and conduction band in QDs. Without adding N atoms, H18, H22, and H23 can achieve 1.30 μm wavelength (corresponding to the transition energies of 954 meV), but H14 cannot, so we can dope 0.60% N atoms into H14 to achieve 1.30 μm wavelength. To achieve the wavelength of 1.55 μm (corresponding to the transition energies of 800 meV), we can dope 2.7% or 2.5% N atoms into H22 and H23 sized QDs, respectively. We will discuss this in details in later parts.

Figure 6(a) shows the transition matrix element of c1-hh1 as a function of QD size for different nitrogen compositions. The presence of nitrogen increases the confinement of the QD electron wave functions compared to equivalent N-free strctures.[28] At the same time, the strong nitrogen–

Author complimentary copy. Redistribution subject to AIP license or copyright, see http://jap.aip.org/jap/copyright.jsp

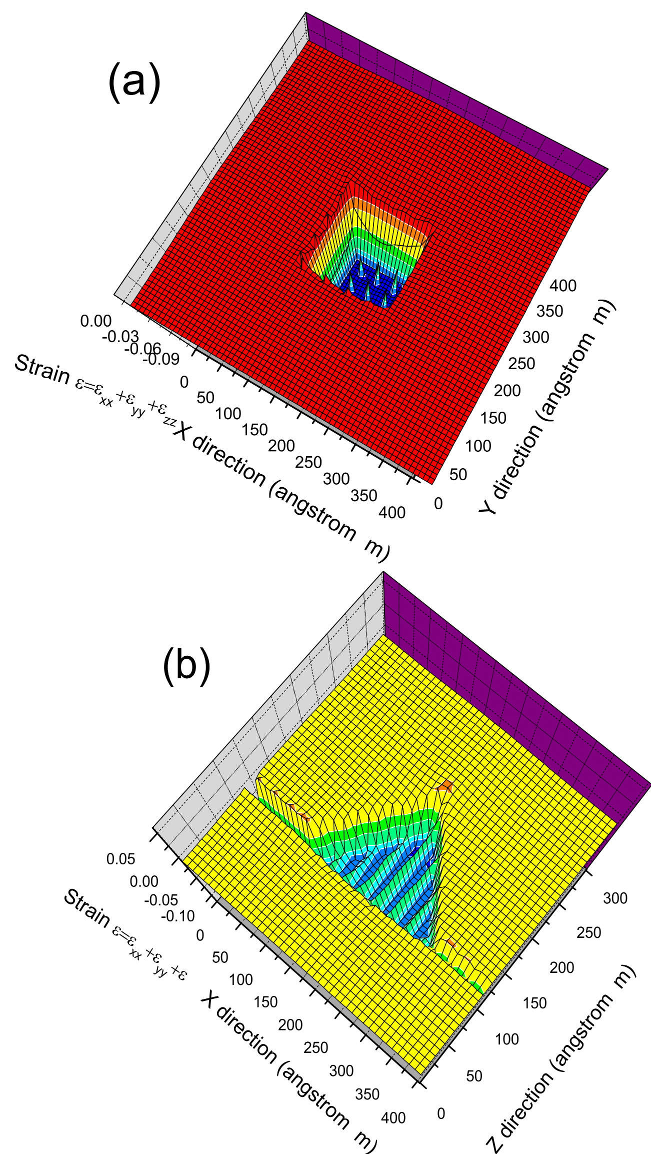

FIG. 4. (Color online) The 3D strain distribution in the unit cell for H18 sized QD with 1% nitrogen composition (a) showing strains in the x-y plane and (b) in the x-z plane with different view angles.

conduction band (N-CB) mixing reduces the QD optical matrix element at the band edge, as a significant part of the electron ground state belongs to the $|s_N\rangle$ character.[29] Because our QDs are assumed to grow along the [001] direction, we do not include piezoelectric effects in our simulation. That may be the reason for the slight difference between our results and Ref. 28. As size increases, for nitrogen-added QD, the electron wave function confinement decreases, but the N-CB mixing decreases resulting reducing the $|s_N\rangle$ character in electron ground state too. Both effects occurs, hence the optimal transition matrix element occurs at different size for different N composition depending on which effect can dominate the other. Figure 6(a) shows the QDs with 1% N reaches its optimal value at smaller size than 2%, and the QDs with 3% N have not reached their optimal value yet. Figure 6(b) shows the transition matrix element of c1-hh1 decreases as N composition increases due to the increasing stronger N-CB mixing,[28] and for smaller QDs, this deceasing is faster. Because c1 energy level is closer to nitrogen resonant level for smaller QD, the N-CB mixing is also stronger. So when N increases, the repulsion interaction increases more significantly.

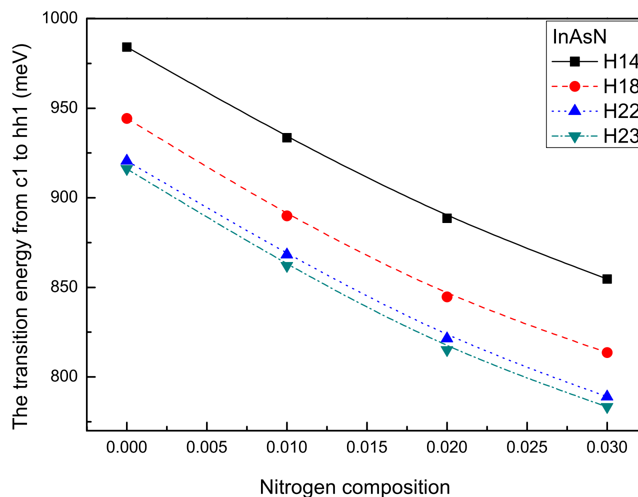

FIG. 5. (Color online) The transition energy from cl (the first excited electron state) to hh1 (the first excited state of heavy hole) as a function of QD height for different nitrogen compositions.

Figure 7 shows the $(\mathrm{fc}+\mathrm{fv}-1)/E$ is a function of carrier

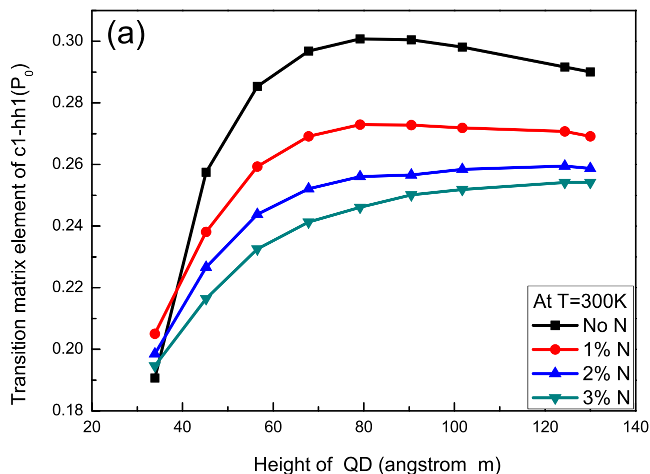

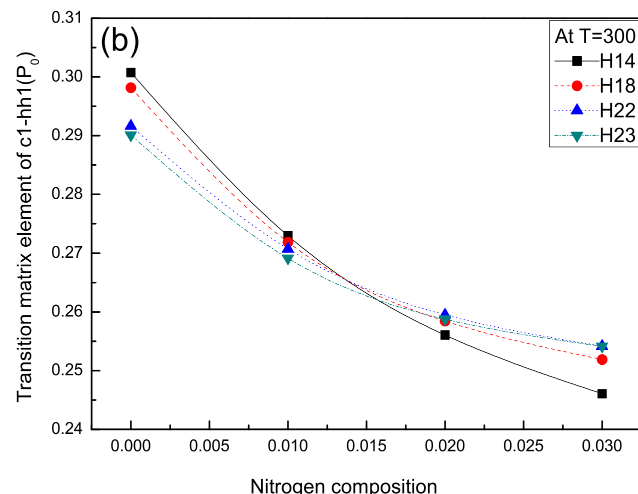

FIG. 6. (Color online) The transition matrix element of c1-hh1 as (a) a function of height of QDs for different N compositions, and (b) a function of nitrogen composition for different sized QDs.

Author complimentary copy. Redistribution subject to AIP license or copyright, see http://jap.aip.org/jap/copyright.jsp

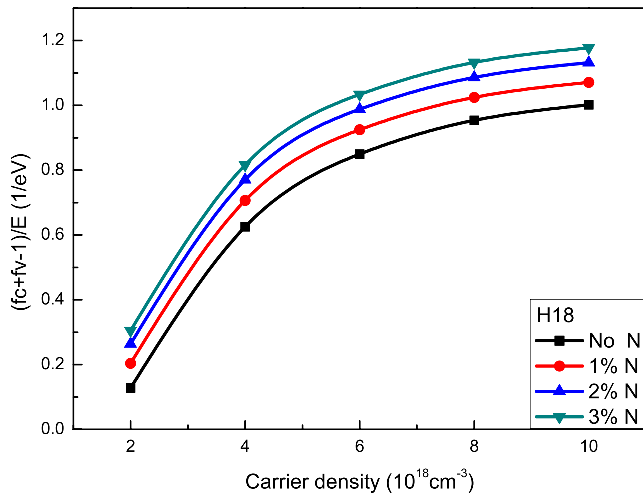

FIG. 7. (Color online) For H18 sized QDs, $(\mathrm{fc}+\mathrm{fv}-1)/E$ is a function of carrier density. E_a is the c1-hh1 transition energy. For different N composition, E_a is different.

density for H18 sized QDs. E is the c1-hh1 transition energy. For H18, E is 944.3 889.9, 844.7, and 816.6 meV for N composition 0%, 1%, 2%, and 3%, respectively. As $(\mathrm{fc}+\mathrm{fv}-1)/E$ is a factor in our gain calculation in Eq. (15), we write it in this form for comparison purpose. Figure 7 shows for different carrier density, the QDs with higher nitrogen composition have high value of $(\mathrm{fc}+\mathrm{fv}-1)/E$. It suggests that fc and fv have greater values for high N, because when more N atoms are added in, the c1 energy level is repulsed to be lower, then the electrons are easier to occupy this first excited state, so the probability to find a electron in c1 increases. This applies to other sized QDs too.

Figure 8 shows the optical gain spectrum for different low nitrogen compositions. We take the QD with H18 sized QD as an example. The optical gain is highly polarized, the TE mode (polarized in the x direction) optical gain is much larger than the TM mode (polarized in the z direction) optical gain, because the strain in QD is compressive. We only show TE mode and neglect TM mode in our figures. For the same

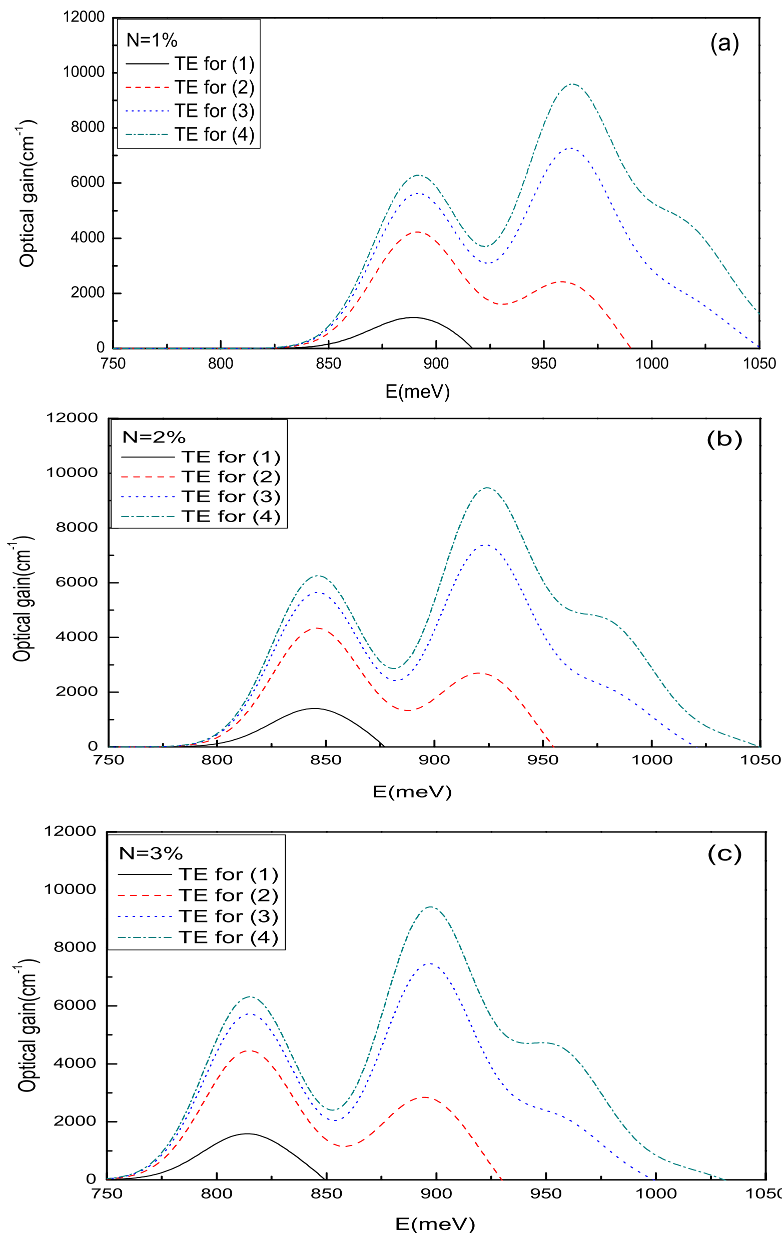

FIG. 8. (Color online) Optical gain vs photon energy for H18 QD with different carrier densities (1) $D=2\times10^{18}$ cm^{-3}; (2) $D=4\times10^{18}$ cm^{-3}; (3) $D=6\times10^{18}$ cm^{-3}; and (4) $D=8\times10^{18}$ cm^{-3}, and different nitrogen compositions (a) N=0.01, (b) N=0.02, (c) N=0.03.

Author complimentary copy. Redistribution subject to AIP license or copyright, see http://jap.aip.org/jap/copyright.jsp

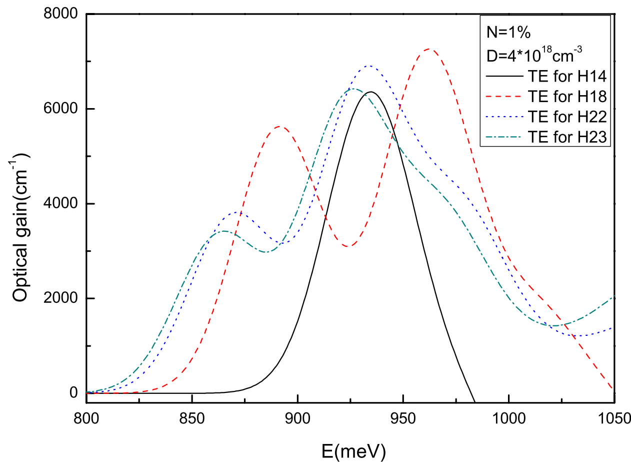

FIG. 9. (Color online) Optical gain for different sized QD with 1% nitrogen composition vs photoenergy for the same carrier density of $D=6\times10^{18}$ cm^{-3}.

N composition, when carrier density increases from 2.0×10^{18} to 8.0×10^{18} cm^{-3}, more and more carriers occupy the higher energy levels, and the first peak (the maximum gain for our concern) denoted as c1-hh1 transition increases, and the second peak appears. This second peak is the higher energy level transition which is undesirable. When N composition increases, the gain spectrum peak shifts to lower photon energy (longer wavelength), mainly due to the band gap decrease. It makes the emission of longer wavelength possible when c1 to hh1 transition occurs. These trends are true for other sized QDs too.

In Fig. 9, we fix the nitrogen composition at 1% and carrier density at 6×10^{18} cm^{-3}, then plot the graph of optical gain for different sized QD. As the size increases from H14 to H23, the first peak transition energy decreases which agrees with Fig. 5. At this N composition and carrier density, H14 has only first peak and H18 has both first and second peaks, but for H22 and H23, their third peak even appears. It agrees with the fact that for larger quantum dots, the energy separation between c1 (the first electron excited state)-c2 (the second electron excited state) and hh1 (the first excited state of heavy hole)-hh2 (the second excited state of heavy hole) are smaller, so the higher excited states transition can easily happen and increase faster. At 1% N composition and the carrier density 6×10^{18} cm^{-3}, H14 has the greatest optical gain.

Next we investigate how the first peak maximum gain varies with carrier density for different nitrogen compositions. In Fig. 10, for each size, we plot the graph of maximum optical gain against carrier density for four different nitrogen compositions. Figures 10(a) and 10(b) show that for smaller QDs, it reaches its saturation gain at very high carrier density. For H14 QDs in Fig. 10(a), when carrier density increases, the optical gain is higher for N-added QDs, it shows the factor of $(\mathrm{fc}+\mathrm{fv}-1)/E$ still dominate over transition matrix element which is decreasing for increasing N. However for H18 QDs in Fig. 10(b), at larger carrier density, the optical gain of N-free QD surpass that with N, it shows the effect of factor $(\mathrm{fc}+\mathrm{fv}-1)/E$ is gradually balanced and overwhelmed by the transition matrix element. In Fig. 7, we can observe that at carrier density 2×10^{18} cm^{-3}, the (fc

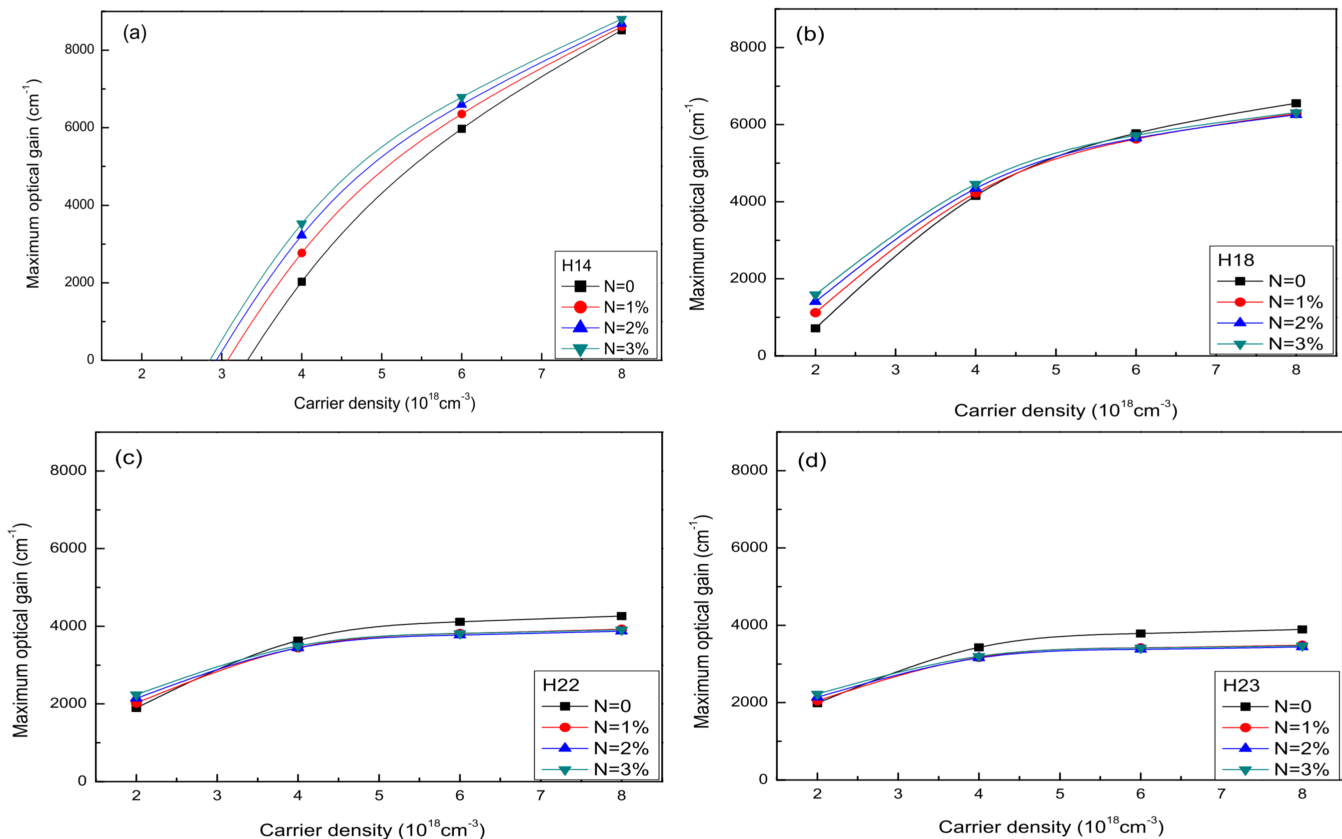

FIG. 10. (Color online) Maximum optical gain vs carrier density for different nitrogen compositions and sizes (a) H14, (b) H18, (c) H22, and (d) H23.

Author complimentary copy. Redistribution subject to AIP license or copyright, see http://jap.aip.org/jap/copyright.jsp

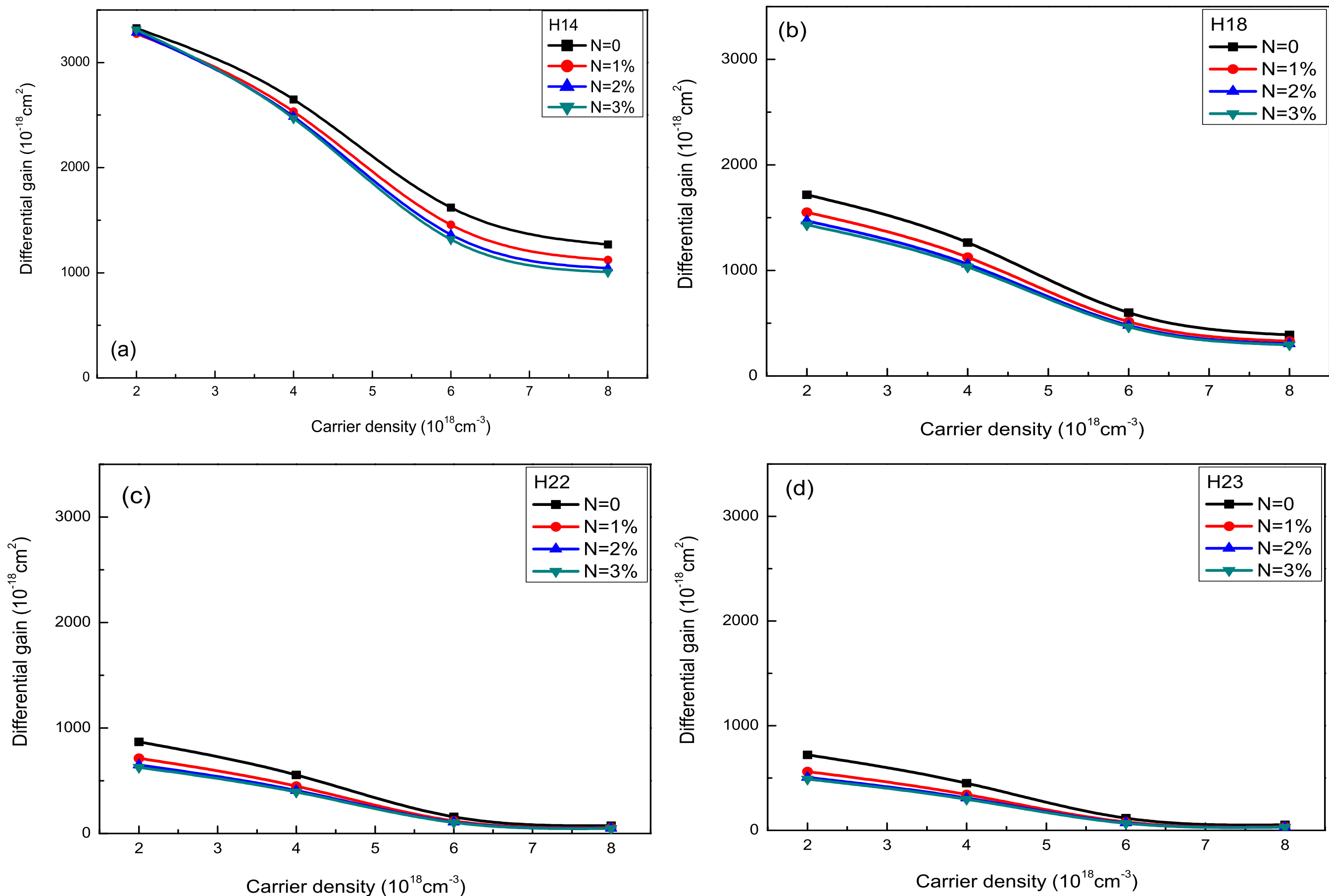

FIG. 11. (Color online) The differential gain for different N composition and size (a) H14, (b) H18, (c) H22, and (d) H23 vs carrier density.

$+fv-1)/E$ for N=3% QD is about 2.4 times of that value for N-free QD. When carrier density increases to 8×10^{18} cm^{-3}, the $(fc+fv-1)/E$ for N=3% QD is about only 1.2 times of that value for N-free QD. It shows the percentage weight of factor $(fc+fv-1)/E$ decreases in the gain calculation. Figures 10(c) and 10(d) show that for larger QDs, it can reach its saturation optical gain in a lower carrier density than smaller QDs, and for different N composition, their saturation gains are almost the same, but smaller than the saturation gain of N-free QD. It suggests that the factor of $(fc+fv-1)/E$ can dominate over the factor of transition matrix element at smaller carrier density for larger QD, and the difference of saturation gain between N-added QD is quite small.

In a semiconductor laser, we are also interested in the differential gain which is $d\text{gain}/dn$ with respect to the carrier density, because the resonant frequency in a semiconductor laser is proportional to the square root of the differential gain with respect to the carrier density.[30] Figure 11 shows the differential gain for different sized QD with different N composition. As QD size increase from H14 to H23, the differential gain drops tremendously, so the QD size should not be too large in order to achieve high resonant frequency. Figure 11(a) shows for smaller QDs, differential gain is not so different at low carrier density, but differential gains drop faster for the QDs with N, resulting the QDs without N has obvious larger differential gain at high carrier density. Figures 11(b)–11(d) show for larger QDs, the differential gain is obvious greater for non-nitrogen QDs at low carrier density, but at high carrier density, the differential gains are all quite low. When we judge the performance of various QD, we should consider its wavelength, initial optical gain, saturation optical gain, and differential gain. So we should choose QD size and nitrogen composition wisely according to the requirement for the applications.

IV. CONCLUSIONS

The electronic structures of InAsN/GaAs QDs are investigated using the ten-band $\mathbf{k}\cdot\mathbf{p}$ model with consideration of the strains and inhomogeneous broadening effect of optical gain due to the size fluctuation of QDs. When more N atoms are added in QD, the repulsion between the resonant energy level of nitrogen atom and c1 increases and c1 is forced to be lower making the reduction in c1-hh1 transition energy. So the long-wavelength emission becomes possible, even 1.55 μm. At the same time, the energy separation between c2-c1 is enlarged, which makes higher excited states combination transition hard to occur. For different sizes of QDs, the strain effect and confinement can significantly affect the energy levels especially conduction band and the optical properties accordingly. To achieve desired lasers for, the trade-off between wavelengths, transparency carrier density, and saturation optical gain must be considered. For the same size QD, when N composition is higher, it can have longer wavelength, higher maximum optical gain, and less detri-

Author complimentary copy. Redistribution subject to AIP license or copyright, see http://jap.aip.org/jap/copyright.jsp

mental effect induced by higher excited state transition. However our simulation is in ideal condition, in real experiment, the higher N composition may cause more N-related defects. The extra N atoms may become nonradiative recombination centers. So depending on the specific application requirements, we should select the N composition and QD size accordingly.

ACKNOWLEDGMENTS

Wei-Jun Fan would like to acknowledge the support from the ASTAR (SERC Grant No. 0621200015) and AcRF RGM 1/07, Jian-Bai Xia would like to acknowledge the support from the National Natural Science Foundation under Grant Nos. 90301007 and 60521001.

[1] A. A. Ukhanov, A. Stintz, P. G. Eliseev, and K. J. Malloy, Appl. Phys. Lett. **84**, 1058 (2004).
[2] O. Schumann, L. Geelhaar, H. Riechert, H. Cerva, and G. Abstreiter, J. Appl. Phys. **96**, 2832 (2004).
[3] J. X. Chen, A. Markus, A. Fiore, U. Oesterle, R. P. Stanley, J. F. Carlin, R. Houdré, M. Ilegems, L. Lazzarini, L. Nasi, M. T. Todaro, E. Piscopiello, R. Cingolani, M. Catalano, J. Katcki, and J. Ratajczak, J. Appl. Phys. **91**, 6710 (2002).
[4] A. E. Zhukov, V. M. Ustinov, A. R. Kovsh, A. Yu. Egorov, N. A. Maleev, N. N. Ledentsov, A. F. Tsatsul'nikov, M. V. Maximov, Yu. G. Musikhin, N. A. Bert, P. S. Kop'ev, D. Bimberg, and Zh. I. Alferov, Semicond. Sci. Technol. **14**, 575 (1999).
[5] M. Sopanen, H. P. Xin, and C. W. Tu, Appl. Phys. Lett. **76**, 994 (2000).
[6] K. C. Yew, S. F. Yoon, and Z. Z. Sun, J. Cryst. Growth **271**, 8 (2004).
[7] S. Tomić, E. P. O'Reilly, P. J. Klar, H. Gruning, W. Heimbrodt, W. M. Chen, and I. A. Buyanova, Phys. Rev. B **69**, 245305 (2004).
[8] S. Kan, T. Mokari, E. Rothenberg, and U. Banin, Nature Mater. **2**, 155 (2003).
[9] S. Tomić, Phys. Rev. B **73**, 125348 (2006).
[10] W. Shan, W. Walukiewicz, J. W. Ager III, E. E. Haller, J. F. Geisz, D. J. Friedman, J. M. Olson, and S. R. Kurtz, Phys. Rev. Lett. **82**, 1221 (1999).
[11] S. Sanguinetti, M. Padovani, M. Gurioli, E. Grilli, M. Guzzi, A. Vinattieri, M. Colocci, P. Frigeri, and S. Franchi, Appl. Phys. Lett. **77**, 1307 (2000).
[12] K. M. Kim, Y. Ju Park, C. H. Roh, Y. M. Park, E. K. Kim, C. K. Hyon, J. Ho Park, and T. W. Kim, Jpn. J. Appl. Phys., Part 1 **42**, 54 (2003).
[13] M. Sugawara, K. Mukai, Y. Nakata, H. Ishikawa, and A. Sakamoto, Phys. Rev. B **61**, 7595 (2000).
[14] C. Pryor, Phys. Rev. B **57**, 7190 (1998).
[15] O. Stier, M. Grundmann, and D. Bimberg, Phys. Rev. B **59**, 5688 (1999).
[16] X. W. Zhang, W. J. Fan, S. S. Li, and J. B. Xia, Appl. Phys. Lett. **90**, 153103 (2007).
[17] Madelung, Landolt-Bornstein, New Series, Group III, Vol. 17, Pt. A, *Semiconductor: Physics of Group IV Elements and III–V Compounds* (Springer, Berlin, 1982), pp. 218 and 318.
[18] S. S. Li, J. B. Xia, Z. L. Yuan, Z. Y. Xu, W. K. Ge, X. R. Wang, Y. Wang, J. Wang, and L. L. Chang, Phys. Rev. B **54**, 11575 (1996).
[19] I. Vurgaftman and J. R. Meyer, J. Appl. Phys. **94**, 3675 (2003).
[20] X. W. Zhang and J. B. Xia, Phys. Rev. B **74**, 075304 (2006).
[21] H. Jiang and J. Singh, Phys. Rev. B **56**, 4696 (1997).
[22] W. H. Press, B. P. Flanner, S. A. Teukolsky, and W. T. Veteering, *Numerical Recipes* (Cambridge University Press, New York, 1989).
[23] C. Pryor, J. Kim, L. W. Wang, A. J. Williamson, and A. Zunger, J. Appl. Phys. **83**, 2548 (1998).
[24] W. J. Fan, M. F. Li, T. C. Chong, and J. B. Xia, J. Appl. Phys. **80**, 3471 (1996).
[25] M. Sugawara, Phys. Rev. B **51**, 10743 (1995).
[26] M. Lorke, W. W. Chow, T. R. Nielsen, J. Seebeck, P. Gartner, and F. Jahnke, Phys. Rev. B **74**, 035334 (2006).
[27] M. Grundmann, N. N. Ledentsov, O. Stier, D. Bimberg, V. M. Ustinov, P. S. Kopv, and Zh. I. Alferov, Appl. Phys. Lett. **68**, 979 (1996).
[28] S. Tomic, Appl. Phys. Lett. **90**, 121115 (2007).
[29] S. Tomic, Phys. Rev. B **73**, 125348 (2006).
[30] S. Tomic, E. P. O'Reilly, R. Fehse, S. J. Sweeney, A. R. Adams, A. D. Andreev, S. A. Choulis, T. J. C. Hosea, and H. Riechert, IEEE J. Sel. Top. Quantum Electron. **9**, 1228 (2003).

Author complimentary copy. Redistribution subject to AIP license or copyright, see http://jap.aip.org/jap/copyright.jsp